

# Absum: Simple Regularization Method for Reducing Structural Sensitivity of Convolutional Neural Networks

Sekitoshi Kanai<sup>1,2</sup>, Yasutoshi Ida<sup>1</sup>, Yasuhiro Fujiwara<sup>3</sup>, Masanori Yamada<sup>4</sup>, Shuichi Adachi<sup>2</sup>

<sup>1</sup>NTT Software Innovation Center <sup>2</sup>Keio University <sup>3</sup>NTT Communication Science Laboratories <sup>4</sup>NTT Secure Platform Laboratories  
{sekitoshi.kanai.fu, yasutoshi.ida.yc, yasuhiro.fujiwara.kh, masanori.yamada.cm}@hco.ntt.co.jp, adachi@appi.keio.ac.jp

## Abstract

We propose Absum, which is a regularization method for improving adversarial robustness of convolutional neural networks (CNNs). Although CNNs can accurately recognize images, recent studies have shown that the convolution operations in CNNs commonly have structural sensitivity to specific noise composed of Fourier basis functions. By exploiting this sensitivity, they proposed a simple black-box adversarial attack: Single Fourier attack. To reduce structural sensitivity, we can use regularization of convolution filter weights since the sensitivity of linear transform can be assessed by the norm of the weights. However, standard regularization methods can prevent minimization of the loss function because they impose a tight constraint for obtaining high robustness. To solve this problem, Absum imposes a loose constraint; it penalizes the absolute values of the summation of the parameters in the convolution layers. Absum can improve robustness against single Fourier attack while being as simple and efficient as standard regularization methods (e.g., weight decay and  $L_1$  regularization). Our experiments demonstrate that Absum improves robustness against single Fourier attack more than standard regularization methods. Furthermore, we reveal that robust CNNs with Absum are more robust against transferred attacks due to decreasing the common sensitivity and against high-frequency noise than standard regularization methods. We also reveal that Absum can improve robustness against gradient-based attacks (projected gradient descent) when used with adversarial training.

## Introduction

Deep neural networks have achieved great success in many applications, e.g., image recognition (He et al. 2016) and machine translation (Vaswani et al. 2017). Specifically, CNNs and rectified linear units (ReLUs) have resulted in breakthroughs in image recognition (LeCun et al. 1989; Nair and Hinton 2010) and are de facto standards for image recognition and other applications (He et al. 2016; Radford, Metz, and Chintala 2016). Though CNNs can classify image data as accurately as humans, they are sensitive to small perturbations of inputs, i.e., injecting imperceptible perturbations can make deep models misclassify image data. Such attacks are called adversarial attacks and the perturbed inputs are called adversarial examples (Szegedy et al. 2013).

We can roughly divide adversarial attacks into two types; white-box attacks, which use the information of target models (Goodfellow, Shlens, and Szegedy 2014; Madry et al. 2018; Moosavi-Dezfooli, Fawzi, and Frossard 2016), and black-box attacks, which do not require the information of target models (Papernot, McDaniel, and Goodfellow 2016; Chen et al. 2017; Papernot et al. 2017). Black-box attacks, rather than white-box attacks, can threaten online deep-learning services since it is difficult to access the target models in online deep-learning applications (Papernot et al. 2017; Yuan et al. 2019).

Most black-box attacks are transferred attacks, which are generated as white-box attacks for substitute models instead of the target model (Papernot, McDaniel, and Goodfellow 2016). This implies that deep models have common sensitivity against specific perturbations. In fact, Tsuzuku and Sato (2019) have recently shown that CNNs have the structural sensitivity from the perspective that convolution can be regarded as the product of the circulant matrix and proposed single Fourier attack (SFA).<sup>1</sup> Fourier basis functions create singular vectors of circulant matrices, and SFA uses these singular vectors since the dominant singular vector can be the worst noise for a matrix-vector product. Although SFA is a very simple attack composed of a single-frequency component, it is universal adversarial perturbations for CNNs, i.e., it can decrease the classification accuracy of various CNN-based models without using the information about the model parameters and without depending on input images. To the best of our knowledge, an effective defense method against SFA has not been proposed. Therefore, such a method is necessary.

To defend CNNs against SFA, we first reveal that the spectral norm constraint (Sedghi, Gupta, and Long 2019) (hereinafter, we call it SNC) can reduce the structural sensitivity. While SNC was proposed to improve generalization performance, it can improve robustness in the Fourier domain since singular values of convolution layers correspond to the magnitude of the frequency response. However, SNC is not so practical since it requires high computational cost to compute the spectral norm (the largest singular value). We then develop *Absum*; an efficient regularization method

<sup>1</sup>Yin et al. (2019) concurrently proposed the same attack.

for reducing the structural sensitivity of CNNs. Instead of the spectral norm, we use the induced  $\infty$ -norm ( $L_\infty$  operator norm) since it is the upper bound of the spectral norm for convolution. However, a constraint of the induced  $\infty$ -norm, which is equivalent to  $L_1$  regularization, requires a tight constraint for robustness, which prevents minimization of the loss function. This is because the induced  $\infty$ -norm is a conservative measure; it handles the effects of negative inputs even though inputs always have positive values after ReLU activations. To improve robustness without preventing the loss minimization, Absum relaxes the induced  $\infty$ -norm by penalizing the absolute values of the summations of weights instead of elements on the basis that input vectors always have positive elements. Absum is as simple as standard regularization methods such as weight decay, but it can reduce sensitivity to SFA. We provide the proximal operator to minimize loss functions with Absum.

Image recognition experiments on MNIST, Fashion-MNIST (FMNIST), CIFAR10, CIFAR100, and SVHN demonstrate that Absum and SNC outperform  $L_1$  and  $L_2$  regularization methods in terms of improving robustness against SFA, and the computation time of Absum is about one-tenth that of SNC. In the additional empirical evaluation, we reveal that robust CNNs against SFA can be robust against transferred attacks by using white-box attacks (projected gradient descent: PGD (Kurakin, Goodfellow, and Bengio 2016; Madry et al. 2018)). This implies that sensitivity to SFA is one of the causes of the transferability of adversarial attacks. As a further investigation of Absum and SNC, we reveal that adversarial perturbations for CNNs trained with Absum and SNC have little high-frequency components, i.e., these CNNs are robust against high-frequency noise. Furthermore, our experiments show that Absum is effective against PGD when using adversarial training.

The following are main contributions of this paper:

- We show that SNC improves robustness against SFA. SNC was proposed to improve generalization performance, but effectiveness in robustness against SFA had not been evaluated.
- We propose Absum and its proximal operator. Absum improves robustness against SFA as well as SNC while its computational cost is lower than that of SNC.
- In the further empirical evaluation, Absum and SNC can also improve robustness against other black-box attacks (transferred attacks and High-Frequency attacks (Wang et al. 2019)). In addition, Absum can improve robustness against PGD when used with adversarial training.

## Preliminaries

### CNNs, ReLUs and Circulant Matrix

In this section, we outline CNNs, ReLUs, and a circulant matrix for convolution operation. Let  $\mathbf{X} \in \mathbf{R}^{n \times n}$  be an input map,  $\mathbf{Y} \in \mathbf{R}^{n \times n}$  be an output map, and  $\mathbf{K} \in \mathbf{R}^{n \times n}$  be a filter matrix such that  $\mathbf{K} = [\mathbf{k}_1, \mathbf{k}_2, \dots, \mathbf{k}_n]^T$ , where  $\mathbf{k}_i = [k_{i,1}, k_{i,2}, \dots, k_{i,n}]^T \in \mathbf{R}^n$ . The output of the convolution operation  $\mathbf{Y} = \mathbf{K} * \mathbf{X}$  becomes

$$Y_{l,m} = \sum_{p=1}^n \sum_{q=1}^n k_{p,q} X_{l+p-1, m+q-1}. \quad (1)$$

Note that when the filter size is  $h \times h$  and  $h < n$ , we can embed it in the  $n \times n$  matrix  $\mathbf{K}$  by padding with zeros (Sedghi, Gupta, and Long 2019). After the convolution, we usually use ReLU activations as the following function:

$$\text{ReLU}(x) = \max(x, 0). \quad (2)$$

Typical model architectures use a combination of convolution and ReLU. For example, a standard block of ResNet (He et al. 2016) is composed as

$$h(\mathbf{X}) = \text{ReLU}(\mathbf{X} + \text{BN}(\mathbf{K}^{(2)} * \text{ReLU}(\text{BN}(\mathbf{K}^{(1)} * \mathbf{X})))), \quad (3)$$

where  $\text{BN}$  is batch normalization (Ioffe and Szegedy 2015).

Since SFA and Absum are based on a circulant matrix for convolution operation, we show that the convolution can be expressed as a product of a vector and doubly block circulant matrix. Let  $\mathbf{x} = \text{vec}(\mathbf{X})$  and  $\mathbf{y} = \text{vec}(\mathbf{Y})$  be vectors obtained by stacking the columns of  $\mathbf{X}$  and  $\mathbf{Y}$ , respectively. Convolution  $\mathbf{K} * \mathbf{X}$  can be written as

$$\mathbf{y} = \mathbf{A}\mathbf{x}, \quad (4)$$

where  $\mathbf{A} \in \mathbf{R}^{n^2 \times n^2}$  is the following matrix:

$$\mathbf{A} = \begin{bmatrix} c(\mathbf{k}_1) & c(\mathbf{k}_2) & \dots & c(\mathbf{k}_n) \\ c(\mathbf{k}_n) & c(\mathbf{k}_1) & \dots & c(\mathbf{k}_{n-1}) \\ \vdots & \vdots & \ddots & \vdots \\ c(\mathbf{k}_2) & c(\mathbf{k}_3) & \dots & c(\mathbf{k}_1) \end{bmatrix}, c(\mathbf{k}_i) = \begin{bmatrix} k_{i,1}, k_{i,2}, \dots, k_{i,n} \\ k_{i,n}, k_{i,1}, \dots, k_{i,n-1} \\ \vdots \\ k_{i,2}, k_{i,3}, \dots, k_{i,1} \end{bmatrix}. \quad (5)$$

The coefficients  $k_{i,j}$  are cyclically shifted in  $c(\mathbf{k}_i) \in \mathbf{R}^{n \times n}$ , and block matrices  $c(\mathbf{k}_i)$  are cyclically shifted in  $\mathbf{A}$ . Therefore,  $\mathbf{A}$  is called a doubly block circulant matrix.

### Single Fourier Attack

As mentioned above, convolution can be written by a doubly block circulant matrix. Such matrices always have eigenvectors  $\mathbf{Q} = \frac{1}{n} \mathbf{F} \otimes \mathbf{F}$ , where elements of  $\mathbf{F}$  are composed of the Fourier basis  $F_{l,m} = \exp(-j \frac{2\pi}{n} lm)$ , where  $j = \sqrt{-1}$  (Jain 1989; Sedghi, Gupta, and Long 2019; Tsuzuku and Sato 2019), and singular vectors are also composed of  $\mathbf{F} \otimes \mathbf{F}$  even if we stack convolution layers (Tsuzuku and Sato 2019; Karner, Schneid, and Ueberhuber 2003). From these characteristics, Tsuzuku and Sato (2019) proposed SFA. The perturbed input image  $\hat{\mathbf{X}}$  by SFA is

$$\hat{\mathbf{X}} = \mathbf{X} + \varepsilon((1+j)(\mathbf{F})_l \otimes (\mathbf{F})_m + (1-j)(\mathbf{F})_{n-l} \otimes (\mathbf{F})_{n-m}), \quad (6)$$

where  $(\mathbf{F})_l \in \mathbf{R}^n$  is the  $l$ -th column vector of  $\mathbf{F}$ ,  $\mathbf{X}$  is an input image, and  $\varepsilon$  is magnitude of the attack. SFA is composed of  $(\mathbf{F})_l \otimes (\mathbf{F})_m$  and its complex conjugate  $(\mathbf{F})_{n-l} \otimes (\mathbf{F})_{n-m}$  to create a perturbation that has real values since inputs of CNNs are assumed to be real values. The  $l$  and  $m$  are hyperparameters such that  $l = 0, 1, \dots, n-1$ ,  $m = 0, 1, \dots, n-1$ . Figure 1 shows examples of CIFAR10 perturbed by SFA. We can see that  $(l, m)$  determines a space-frequency of the noise. Note that stacked convolution layers without activation functions (e.g.,  $\mathbf{A}^{(2)}\mathbf{A}^{(1)}\mathbf{x}$ ) also have singular vectors composed of Fourier basis functions. Even though we use nonlinear activation functions, many model architectures (e.g., WideResNet, DenseNet-BC, and GoogLeNet) are sensitive to SFA (Tsuzuku and Sato 2019).

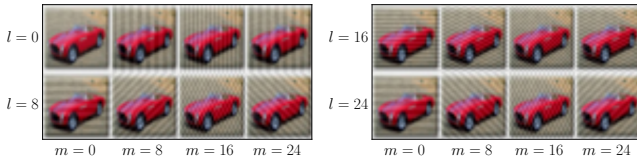


Figure 1: Examples perturbed by SFA of  $(l, m) = (0, 0), (0, 8), \dots, (24, 16), (24, 24)$

## Vulnerability of CNNs in Frequency Domain

Sensitivity to SFA can be regarded as sensitivity to a single-frequency noise (Yin et al. 2019). To understand the vulnerability of CNNs, several studies focused on sensitivity of CNNs in the frequency domain (Yin et al. 2019; Wang et al. 2019; Das et al. 2018; Liu et al. 2019). These studies point out that sensitivity to high-frequency components in images is one of the causes of adversarial attacks since human visual systems are not sensitive to high-frequency components unlike CNNs. In fact, several studies show that CNNs are sensitive to high-frequency noise (Jo and Bengio 2017; Wang et al. 2019; Yin et al. 2019; Das et al. 2018). Jo and Bengio (2017) and Wang et al. (2019) show that CNNs misclassify images processed by low-pass filters and Wang et al. (2019) call this a High-Frequency attack, which is a simple black-box adversarial attack. There is a hypothesis that robust CNNs against high-frequency noise are also robust against adversarial attacks (Wang et al. 2019; Yin et al. 2019). Note that Wang et al. (2019) claimed that sensitivity in the high-frequency domain contributes to high performance on clean data; thus, there is a trade-off.

## Related Work

Adversarial attacks can be transferred to other models and transferred white-box attacks become adversarial black-box attacks (Papernot et al. 2017). These attacks can be defended against by adversarial training, which is a promising defense method (Papernot et al. 2017; Madry et al. 2018). However, the computational cost of adversarial training is larger than naive training. Note that Absum can be used with adversarial training. Several studies proposed black-box attacks using queries to ask the target model about predicted labels of given data, but these attacks might still be impractical since they require many queries (Chen et al. 2017; Brendel, Rauber, and Bethge 2018; Ilyas et al. 2018). On the other hand, SFA only uses the information that the target model is composed of CNNs and is more practical.

Our method simply penalizes parameters in a similar manner compared to standard regularization methods. As standard regularization methods,  $L_2$  regularization (weight decay) is commonly used for improving generalization performance due to its simplicity.  $L_1$  regularization is also used since it induces sparsity (Goodfellow, Bengio, and Courville 2016). In addition, spectral norm (induced 2-norm) regularization can also improve generalization performance (Yoshida and Miyato 2017; Sedghi, Gupta, and Long 2019). Due to space limitations, we outline other studies less relevant than the above studies in the appendix.

## Defense Methods against SFA

In this section, we first show that SNC can improve robustness against SFA. Since SNC has a large time complexity, we next discuss whether standard regularizations can be alternatives. Finally, we discuss Absum and its proximal operator, which is an efficient defense method against SFA.

## Spectral Norm Constraint

SFA is based on the following properties of linear transform:

$$\sigma(\mathbf{A}) = \max_{\|\mathbf{x}\|_2=1} \|\mathbf{Ax}\|_2, \quad \mathbf{v} = \arg \max_{\|\mathbf{x}\|_2=1} \|\mathbf{Ax}\|_2, \quad (7)$$

where  $\sigma$  is the largest singular value (spectral norm or induced 2-norm), and  $\mathbf{v}$  is the right singular vector corresponding to  $\sigma$ . Equation (7) shows that the singular vector can be the worst noise for linear transform, and SFA uses the singular vectors for convolutional layers. Since the spectral norm determines the impact of SFA, we can reduce sensitivity to SFA by constraining the spectral norm. The constraint of the spectral norm for CNNs (i.e., SNC) (Sedghi, Gupta, and Long 2019; Gouk et al. 2018) was proposed in the context of improving generalization performance. SNC clips  $\sigma$  if it exceeds a preset threshold; thus, it can directly control sensitivity to a single-frequency perturbation. However, the constraints of the exact spectral norm<sup>2</sup> of  $\mathbf{A}$  incurs large computation cost; the  $O(n^2c^2(c + \log(n)))$  time for each convolution when input size is  $n \times n$ , and the numbers of input and output channels are  $c$  even if we use the efficient spectral norm constraints (Sedghi, Gupta, and Long 2019). SNC can be infeasible when the size of inputs increases.

## Standard Regularizations fail to Defend

Instead of using the spectral norm, we can assess the effect of the perturbation for linear transform by using

$$\max_{\|\mathbf{x}\|_\infty=1} \|\mathbf{Ax}\|_\infty. \quad (8)$$

Equation (8) is the induced  $\infty$ -norm  $\|\mathbf{A}\|_\infty$ , and we have  $\|\mathbf{A}\|_2 \leq \|\mathbf{A}\|_\infty$  for convolution (it is proved in the appendix). This norm is calculated as:

$$\|\mathbf{A}\|_\infty = \max_l \sum_m |A_{l,m}|. \quad (9)$$

Substituting eq. (5) for eq. (9), we have

$$\max_l \sum_m |A_{l,m}| = \sum_m \sum_l |k_{l,m}|. \quad (10)$$

Thus, the penalty of the induced  $\infty$ -norm can be  $L_1$  regularization (Gouk et al. 2018). Therefore,  $L_1$  regularization can improve robustness. However, the induced  $\infty$ -norm is a conservative measure of robustness (Szegedy et al. 2013); the highly weighted  $L_1$  regularization for robustness can prevent minimization of the loss function. Figure 2 shows the test accuracy of models, which is trained with  $L_1$  regularization, on data perturbed by SFA against the regularization weight  $\lambda$ . In this figure, the robust accuracy against SFA increases along with the regularization weight, i.e., the robustness increases according to the regularization weight. However, the

<sup>2</sup>The spectral norm in spectral norm regularization (Yoshida and Miyato 2017) is often quite different from that of  $\mathbf{A}$  (Sedghi, Gupta, and Long 2019; Gouk et al. 2018).

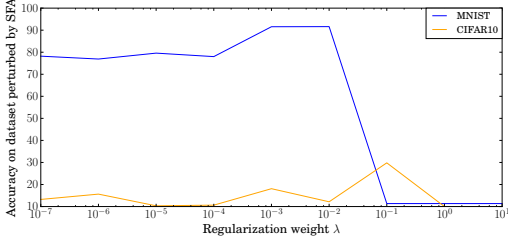


Figure 2: Accuracy of models trained with  $L_1$  regularization on test dataset perturbed by SFA vs regularization weight.  $l, m$  of SFA are tuned to minimize accuracy for each  $\lambda$ .

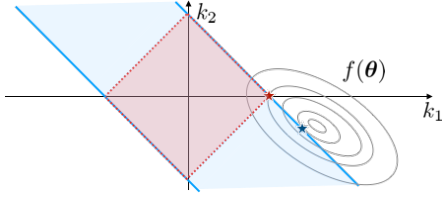


Figure 3: Comparison of search spaces of Absum:  $|k_1 + k_2|$  (blue) and  $L_1$  regularization:  $|k_1| + |k_2|$  (red) where  $f(\theta)$  is loss function. We have  $\{\mathbf{k} \mid \sum_i |k_i| \leq c\} \subseteq \{\mathbf{k} \mid |\sum_i k_i| \leq c\}$  for any constant  $c \geq 0$  from triangle inequality.

accuracy significantly decreases when the weight exceeds a certain point. This is because training with high weighted  $L_1$  regularization does not have sufficient search space to minimize the loss function. Note that weight decay can also penalize the spectral norm (in the appendix) and imposes tight regularization, as discussed in the experiments section. Therefore, we need a weak regularization method such that models become both highly robust and accurate.

### Absum: Simple and Weak Regularization

To develop a weak regularization method, we reconsider the optimization problem of eq. (8). The maximum point (eq. (9)) is achieved by  $x_m = \text{sign}(A_{l',m})$ , where  $l' = \arg \max_l \sum_m |A_{l,m}|$ , i.e.,  $x_m = 1$  if  $A_{l',m} > 0$  and  $x_m = -1$  if  $A_{l',m} < 0$ . However, we should consider the sign of input in practice because we usually use ReLUs as activation functions. As described in eq. (3), ReLUs are used before convolution as  $\mathbf{K} * \text{ReLU}(\cdot)$ . Thus,  $\mathbf{x}$  cannot have negative elements, i.e.,  $x_m$  cannot be  $\text{sign}(A_{l',m})$  when  $\text{sign}(A_{l',m}) = -1$ . Therefore, the induced  $\infty$ -norm can overestimate sensitivity to the perturbation. From this insight, we consider the norm of  $\mathbf{A}\mathbf{x}$  when  $\mathbf{x} = \mathbf{1}$  instead of eq. (8)

$$\|\mathbf{A}\mathbf{1}\|_\infty = \max_l \left| \sum_m A_{l,m} \right| = \left| \sum_m \sum_l k_{l,m} \right|. \quad (11)$$

For robustness, we use this value as the regularization term. We call our method *Absum* since this value is the absolute value of the summation of the filter coefficients.

The objective function of training with Absum is

$$\min_{\theta} \frac{1}{N} \sum_{p=1}^N f(\theta, \mathbf{X}_p, \mathbf{Y}_p) + \lambda \sum_{i=1}^L g(\mathbf{K}^{(i)}), \quad (12)$$

$$g(\mathbf{K}^{(i)}) = \left| \sum_{m=1}^n \sum_{l=1}^n k_{l,m}^{(i)} \right|,$$

where  $f(\cdot)$  is a loss function,  $\mathbf{X}_p$  and  $\mathbf{Y}_p$  are the  $p$ -th training image and label, respectively,  $\theta$  is the parameter vector including  $\mathbf{K}^{(i)}$  in the model, and  $\lambda$  is a regularization weight. The  $\mathbf{K}^{(i)}$  is the filter matrix of the  $i$ -th convolution, and  $L$  is the number of convolution filters.<sup>3</sup> Figure 3 shows search spaces of Absum (blue) and  $L_1$  regularization (red) when we have two parameters. The constraint of Absum is looser than  $L_1$  regularization because a large element  $k_{l,m}^{(i)} \gg 0$  is allowed if a small element  $k_{l',m'}^{(i)} \ll 0$  satisfies  $|k_{l,m}^{(i)}| = |k_{l',m'}^{(i)}|$ . Even if  $|\sum_l \sum_m k_{l,m}| = 0$ , the search space of Absum is a  $n^2 - 1$  dimensional space  $\{\mathbf{K} \mid \mathbf{K} \in \mathbf{R}^{n \times n}, \sum_l \sum_m k_{l,m} = 0\}$  while that of  $L_1$  regularization is a point  $\mathbf{K} = \mathbf{O}$  if  $\sum_l \sum_m |k_{l,m}| = 0$ . Note that the search space of weight decay is also the point  $\mathbf{K} = \mathbf{O}$  when  $\|\mathbf{K}\|_F = 0$ . Therefore, the loss function with Absum can be lower than that with  $L_1$  regularization and weight decay if we use a large  $\lambda$ .

Note that when the filter size is  $h \times h$  and  $h < n$ , we only need to compute  $|\sum_{m=1}^h \sum_{l=1}^h k_{l,m}|$  since zeros padded in  $\mathbf{K}$  do not affect eq. (12) (hereafter, we use  $h$  instead of  $n$ ).

### Proximal Operator for Absum

Since  $g(\mathbf{K})$  is not differentiable at  $\sum_l \sum_m k_{l,m} = 0$ , the gradient method might not be effective for minimizing eq. (12). To minimize eq. (12), we use a proximal gradient method, which can minimize a differentiable loss function with a non-differentiable regularization term (Parikh, Boyd, and others 2014). We now introduce proximal operator for Absum. For clarity, let  $\bar{\mathbf{k}}$  be  $\bar{\mathbf{k}} = \text{vec}(\mathbf{K}) = [k_0^T, \dots, k_{h-1}^T]^T \in \mathbf{R}^{h^2}$ . The proximal operator for  $\lambda g(\bar{\mathbf{k}})$  is

$$\text{prox}_{\lambda g}(\bar{\mathbf{k}}) = \begin{cases} \bar{\mathbf{k}} + \lambda \mathbf{1} & \text{if } \sum_l \sum_m k_{l,m} < -h^2 \lambda, \\ \bar{\mathbf{k}} - \frac{\sum_l \sum_m k_{l,m}}{h^2} \mathbf{1} & \text{if } -h^2 \lambda \leq \sum_l \sum_m k_{l,m} \leq h^2 \lambda, \\ \bar{\mathbf{k}} - \lambda \mathbf{1} & \text{if } \sum_l \sum_m k_{l,m} > h^2 \lambda. \end{cases} \quad (13)$$

The following lemmas show that eq. (13) is the proximal operator for Absum:

**Lemma 1.** If  $\bar{\mathbf{k}} = [\bar{k}_1, \dots, \bar{k}_n]^T \in \mathbf{R}^n$ ,  $g(\bar{\mathbf{k}}) = |\sum_i \bar{k}_i|$  is a convex function.

**Lemma 2.** If  $\bar{\mathbf{k}} = [\bar{k}_1, \dots, \bar{k}_n]^T \in \mathbf{R}^n$ ,  $\mathbf{u} \in \mathbf{R}^n$  and  $g(\bar{\mathbf{k}}) = |\sum_i \bar{k}_i|$ , we have

$$\text{prox}_{\lambda g}(\bar{\mathbf{k}}) = \arg \min_{\mathbf{u}} \frac{1}{2} \|\mathbf{u} - \bar{\mathbf{k}}\|_2^2 + \lambda \left| \sum_i u_i \right| \quad (14)$$

$$= \begin{cases} \bar{\mathbf{k}} + \lambda \mathbf{1} & \text{if } \sum_i \bar{k}_i < -n\lambda, \\ \bar{\mathbf{k}} - \frac{\sum_i \bar{k}_i}{n} \mathbf{1} & \text{if } -n\lambda \leq \sum_i \bar{k}_i \leq n\lambda, \\ \bar{\mathbf{k}} - \lambda \mathbf{1} & \text{if } \sum_i \bar{k}_i > n\lambda. \end{cases} \quad (15)$$

The proofs of lemmas are provided in the appendix. Lemma 1 shows that we can use the proximal gradient method, and Lemma 2 shows that the proximal operator of Absum can be obtained as the closed-form of eq. (15). By using the proximal operator after stochastic gradient descent (SGD), we update the  $i$ -th convolution filter:

$$\bar{\mathbf{k}}^{(i)} \leftarrow \text{prox}_{\eta \lambda g}(\bar{\mathbf{k}}^{(i)} - \eta \nabla_{\bar{\mathbf{k}}^{(i)}} \frac{1}{B} \sum_{b=1}^B f(\theta, \mathbf{X}_b, \mathbf{Y}_b)) \quad (16)$$

<sup>3</sup>We penalize the filter matrix for each channel. If one convolution layer has  $c_1$  output channels and  $c_2$  input channels, the regularization term becomes  $\lambda \sum_{l=1}^{c_1} \sum_{m=1}^{c_2} g(\mathbf{K}^{(l+(m-1)c_1)})$ .

where  $\eta$  is a learning rate, and  $B$  is a minibatch size. We provide the pseudocode of the whole training in the appendix. We can compute the proximal operator in  $O(h^2)$  time for each convolution when the filter size is  $h \times h$  because we only need to compute the summation of parameters and elementwise operations. We can also compute weight decay and  $L_1$  regularization in  $O(h^2)$  since the number of parameters in each convolution is  $h^2$ . Therefore, the order of computational complexity of Absum is the same as those of weight decay and  $L_1$  regularization. When we have  $c$  input channels and  $c$  output channels, the computational costs of Absum, weight decay, and  $L_1$  regularization are  $O(c^2h^2)$  and less than that of SNC ( $O(c^2n^2(c+\log(n)))$ ) where  $n \geq h$ .

Note that the loss function  $f$  for training deep neural networks is usually non-convex while  $g(\mathbf{K})$  is convex. Several studies investigate the proximal gradient method when  $f$  is non-convex (Li and Lin 2015), and Wen et al. (2016) use the proximal gradient method for inducing sparse structures in deep learning. We observed that the algorithm of Absum can find a good parameter point during the experiments.

## Experiments

We discuss the evaluation of the effectiveness of SNC and Absum in improving robustness against SFA. Next, we show that Absum is more efficient than SNC especially when the size of input images and models are large. Finally, as the further investigation, we discuss the evaluation of the performance of Absum and SNC in terms of robustness against transferred attacks, vulnerability in frequency domain, and robustness against PGD when used with adversarial training. To evaluate effectiveness, we conducted experiments of image recognition on MNIST (LeCun et al. 1998), FMNIST (Xiao, Rasul, and Vollgraf 2017), CIFAR10, CIFAR100 (Krizhevsky and Hinton 2009), and SVHN (Netzer et al. 2011). We compared Absum and SNC with standard regularizations (weight decay (WD) and  $L_1$  regularization).

### Experimental Conditions

We provide details of the experimental conditions in the appendix. In all experiments, we selected the best regularization weight from among  $[10^1, 10^0, \dots, 10^{-7}]$  for Absum and standard regularization methods, and the best spectral norm  $\sigma$  from among  $[0.01, 0.1, 0.5, 1.0, 10]$  for SNC. In SNC, we clipped  $\sigma$  once in 100 iterations due to the large computational cost. For MNIST and FMNIST, we stacked two convolutional layers and two fully connected layers and used ReLUs as activation functions. For CIFAR10, CIFAR100, and SVHN, the model architecture was ResNet-18 (He et al. 2016). We used SFA with  $l, m \in \{0, 1, \dots, 27\}$  and  $\varepsilon = 80/255$  on MNIST and FMNIST, and  $l, m \in \{0, 1, \dots, 31\}$  and  $\varepsilon = 10/255$  on CIFAR10, CIFAR100, and SVHN.

In addition, we used PGD to evaluate robustness against transferred attacks and white-box attacks since PGD is a sophisticated white-box attack. In addition to naive training, we evaluated robustness against PGD when we used adversarial training (Kurakin, Goodfellow, and Bengio 2016; Madry et al. 2018) with each method because Absum can

be used with it due to its simplicity. Model architectures were the same as in the experiments involving SFA. The hyperparameter settings for PGD were based on (Madry et al. 2018). The  $L_\infty$  norm of the perturbation  $\varepsilon$  was set to  $\varepsilon = 0.3$  for MNIST and FMNIST and  $\varepsilon = 8/255$  for CIFAR10, CIFAR100, and SVHN at training time. For PGD, we updated the perturbation for 40 iterations with a step size of 0.01 on MNIST and FMNIST at training and evaluation times, and on CIFAR10, CIFAR100, and SVHN, for 7 iterations with a step size of  $2/255$  at training time and 100 iterations with the same step size at evaluation time.

### Effectiveness and Efficiency

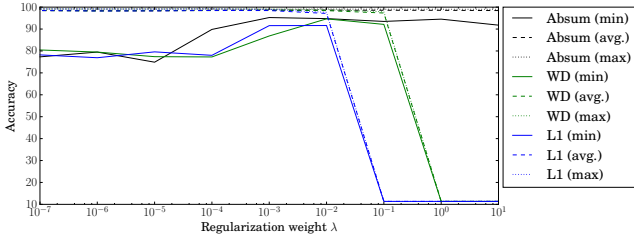
**Robustness against SFA** Table 1 lists the accuracies of each method on test data perturbed by SFA and selected  $\lambda$  and  $\sigma$ . In this table, Avg. denote robust accuracies against SFA averaged over  $(l, m)$ , and Min. denotes minimum accuracies among hyperparameters  $(l, m)$ , i.e., robust accuracies against optimized SFA. CLN denotes accuracies on clean data. The  $\lambda$  and  $\sigma$  are selected so that Avg. would become the highest. In Tab. 1, Absum and SNC are more robust against SFA compared with WD and  $L_1$ . Although SNC is more robust than Absum on CIFAR10 and CIFAR100, clean accuracies of SNC are less than those of Absum and the computation time of SNC is larger than that of Absum as discussed below. In the appendix, we provide accuracies against each  $(l, m)$  and the results in which  $\lambda$  and  $\sigma$  are selected so that each of CLN and Min. would become highest.

Figure 4 shows the test accuracies of the methods on MNIST and CIFAR10 perturbed by SFA against regularization weights. In this figure, min and max denote the minimum and maximum test accuracies among  $(l, m)$ , respectively, and avg. denotes test accuracies averaged over  $(l, m)$ . All methods tend to increase their minimum accuracy (results of SFA with optimized  $(l, m)$ ) according to the regularization weight. However,  $L_1$  and WD significantly decrease in accuracy when the regularization weight is higher than  $10^{-1}$ . On the other hand, Absum with the high regularization weight does not decrease in accuracy. Figure 5 shows the lowest training loss  $\frac{1}{N} \sum f$  in training on CIFAR10 against  $\lambda$ . WD and  $L_1$  with a large  $\lambda$  prevent minimization of the training loss. On the other hand, Absum with a large  $\lambda$  can decrease the training loss because the search space of  $\mathbf{K}^{(i)} \in \mathbf{R}^{h \times h}$  has  $h^2 - 1$  dimensional space even if  $g(\mathbf{K}^{(i)}) = 0$ . In conclusion, standard regularization methods might not be effective in improving robustness against SFA because the high regularization weight imposes too tight of constraints to minimize the loss function. On the other hand, Absum imposes looser constraints; thus, we can improve robustness while maintaining classification performance. The results of other datasets are almost the same as Fig. 4 (included in the appendix). We also provide figures showing the accuracy and the training loss of SNC against  $\sigma$  in the appendix.

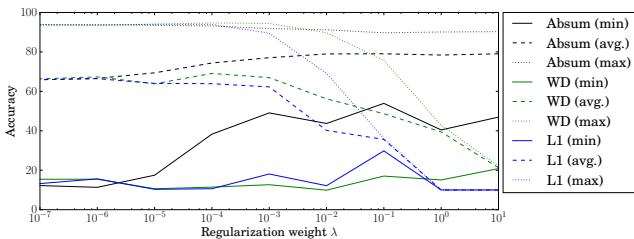
**Computational Cost** To confirm the efficiency of Absum, we evaluated the runtime for one epoch. We also evaluated the runtime of the forward and backward processes of ResNet-18 for one image when input size increases by

Table 1: Accuracies on datasets perturbed by SFA.

	Avg.				Min.				CLN				$\lambda$ and $\sigma$			
	Absum	WD	L1	SNC	Absum	WD	L1	SNC	Absum	WD	L1	SNC	Absum	WD	L1	SNC
MNIST	<b>98.64</b>	98.59	98.48	98.55	<b>94.76</b>	86.84	78.01	91.79	99.14	99.10	<b>99.18</b>	99.10	$10^{-2}$	$10^{-3}$	$10^{-4}$	10
FMNIST	<b>83.11</b>	83.09	82.49	82.60	<b>60.12</b>	47.57	58.38	55.36	<b>88.46</b>	86.99	87.05	87.50	$10^{-3}$	$10^{-2}$	$10^{-3}$	10
CIFAR10	79.05	69.09	66.44	<b>85.57</b>	53.90	11.44	15.64	<b>73.99</b>	89.69	<b>94.73</b>	<b>93.41</b>	88.37	$10^{-1}$	$10^{-4}$	$10^{-6}$	0.5
CIFAR100	48.69	42.97	38.99	<b>60.42</b>	16.32	5.23	9.84	<b>45.05</b>	68.72	67.05	<b>71.68</b>	62.76	$10^{-3}$	$10^{-6}$	$10^{-7}$	1
SVHN	<b>93.34</b>	91.74	91.14	93.20	<b>73.69</b>	60.36	57.52	62.90	95.93	<b>96.37</b>	96.20	95.42	$10^{-3}$	$10^{-3}$	$10^{-7}$	0.1



(a) MNIST



(b) CIFAR10

Figure 4: Accuracy on test datasets perturbed by SFA vs  $\lambda$

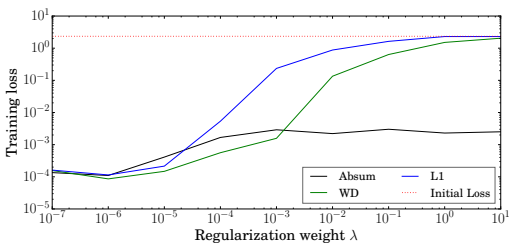
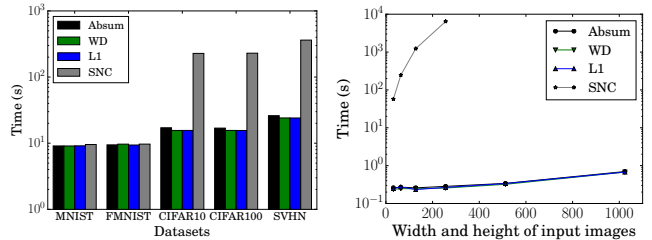


Figure 5: Training loss vs  $\lambda$

using random synthetic three channels images whose sizes were  $32 \times 32$ ,  $64 \times 64$ ,  $128 \times 128$ ,  $256 \times 256$ ,  $512 \times 512$ , and  $1024 \times 1024$  with 10 random labels. The results are shown in Fig. 6. As shown in Fig. 6 (a), Absum is about ten times faster than SNC on  $32 \times 32$  image datasets with ResNet18. The runtime of SNC is comparable to those of other methods on MNIST and FMNIST because we use only two convolution layers, and image sizes of these datasets are smaller than other datasets. In Fig. 6 (b), the runtime of Absum does not increase significantly compared with SNC and the increase in the runtime of Absum is similar to those of standard regularization methods. This is because the computational cost of Absum does not depend on the size of input images. Since SNC incurs large computational cost and depends on the in-



(a) Runtime for one epoch

(b) Runtime vs. input size

Figure 6: Computation time

Table 2: Robust accuracy against transferred PGD attacks. Results of other  $\varepsilon$  are shown in the appendix. w/o Reg. denotes results of training without regularization.

	Absum	WD	L1	SNC	w/o Reg.
MNIST ( $\varepsilon = 0.2$ )	<b>76.34</b>	48.94	66.48	71.30	65.87
FMNIST ( $\varepsilon = 0.2$ )	<b>30.08</b>	3.46	18.35	21.31	19.74
CIFAR10 ( $\varepsilon = 4/255$ )	26.29	18.48	15.66	<b>48.85</b>	15.85
CIFAR100 ( $\varepsilon = 4/255$ )	18.57	17.40	16.68	<b>36.57</b>	16.68
SVHN ( $\varepsilon = 4/255$ )	49.11	40.49	52.79	46.36	<b>54.39</b>

put size, we could not evaluate the runtime when the image width is larger than 256.

## Extensive Empirical Investigation

**Robustness against Transferred Attacks** Sensitivity to SFA is caused by convolution operation and is universal for CNNs. This sensitivity might be a cause of transferability of adversarial attacks, and robust CNNs against SFA can be robust against transferred attacks. To confirm this hypothesis, we investigate sensitivity to transferred PGD. We generate adversarial examples by using the substitute models that were trained under the same setting as that presented in the previous section but with different random initializations. We used these substitute models rather than completely different models because they can be regarded as one of the worst-case instances for transferred attacks (Madry et al. 2018). The accuracies on these adversarial examples are listed in Tab. 2. Absum and SNC improve robustness compared to WD and  $L_1$ . Tables 1 and 2 imply that the method of improving robustness against SFA can also improve robustness against the transferred attacks. This is the first study that shows the relation between robustness against SFA and against transferred white-box attacks.

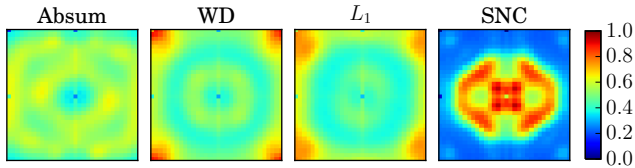


Figure 7: Power spectra of PGD perturbations on CIFAR10. Magnitudes in low-frequency and high-frequency domains are located near center and edge of each figure, respectively. They are normalized as in (0, 1) after logarithmic transform.

Table 3: Robust accuracy against High-Frequency attacks.

	Absum	WD	L1	SNC	w/o Reg.
MNIST	99.00	98.98	<b>99.10</b>	98.97	99.01
FMNIST	84.15	83.91	82.56	<b>84.30</b>	84.03
CIFAR10	64.51	52.82	47.01	<b>82.11</b>	47.46
CIFAR100	41.44	36.15	31.53	<b>61.22</b>	31.80
SVHN	<b>52.95</b>	28.11	17.03	18.75	11.13

**Sensitivity in Frequency Domain** Several studies show that CNNs are sensitive to high-frequency noise unlike human visual systems since CNNs are biased towards high-frequency information (Wang et al. 2019; Yin et al. 2019). From the robustness against SFA, which is regarded as single-frequency noise, Absum and SNC can be expected not to bias CNNs towards high-frequency information. To confirm this hypothesis, we first investigate the power spectra of adversarial perturbations of models trained using each method. Next, we investigate robustness against High-Frequency attacks, which remove high-frequency components of image data. High-Frequency attacks have a hyper-parameter of radius that determines the cutoff frequency, and we set it as half the image width. In these experiments,  $\lambda$  and  $\sigma$  are the same as those in Tab. 1.

Figure 7 shows the power spectra of PGD perturbations on CIFAR10 and Tab. 3 lists the accuracies on the test data processed by High-Frequency attacks. In Fig. 7, we shift low frequency components to the center of the spectrum and power spectra are averaged over test data and RGB channels. This figure shows that vulnerabilities of WD and  $L_1$  are biased in the high-frequency domain, while vulnerability of SNC is highly biased in the low-frequency domain. The power spectrum of Absum is not biased towards a specific frequency domain. Due to these characteristics, SNC and Absum are more robust against High-Frequency attacks than WD and  $L_1$  (Tab. 3). Since human visual systems can perceive low-frequency noise better than high-frequency noise, attacks for Absum and SNC might be more perceptible than attacks for WD and  $L_1$ . Note that Absum is more robust against high-pass filtering than SNC, which is presented in the appendix. This result supports that Absum does not bias CNNs towards a specific frequency domain while SNC biases CNNs towards the low-frequency domain.

**Robustness against PGD with Adversarial Training** Table 4 lists the accuracies of models trained by adversarial training on data perturbed by PGD. When using adversarial

Table 4: Accuracies (%) on test datasets perturbed by PGD.

MNIST		Adversarial training					
$\epsilon$	0.05	0.10	0.15	0.20	0.25	0.30	
Absum $\lambda = 10^{-3}$	<b>96.01</b>	<b>94.92</b>	<b>93.75</b>	<b>92.73</b>	<b>91.59</b>	<b>90.78</b>	
WD $\lambda = 10^{-4}$	92.97	91.34	89.69	88.02	87.05	85.96	
L1 $\lambda = 10^{-4}$	93.12	91.86	90.60	89.28	88.25	87.06	
SNC $\sigma = 10$	91.92	89.43	86.77	83.89	80.24	76.92	
w/o Reg.	91.57	89.85	88.43	86.87	85.76	84.86	
FMNIST		Adversarial training					
Absum $\lambda = 10^{-3}$	<b>66.94</b>	<b>65.92</b>	<b>65.77</b>	<b>65.52</b>	<b>65.24</b>	<b>64.95</b>	
WD $\lambda = 10^{-5}$	65.38	63.64	62.91	62.60	62.11	61.96	
L1 $\lambda = 10^{-6}$	66.13	64.16	62.95	62.23	61.64	61.66	
SNC $\sigma = 10$	51.58	49.33	47.31	45.85	44.86	44.04	
w/o Reg.	63.36	61.66	61.15	60.97	60.46	60.26	
CIFAR10		Adversarial training					
$\epsilon$	4/255	8/255	12/255	16/255	20/255		
Absum $\lambda = 10^{-5}$	69.42	49.39	<b>30.22</b>	<b>15.03</b>	<b>6.54</b>		
WD $\lambda = 10^{-5}$	<b>69.48</b>	49.38	29.37	14.45	6.06		
L1 $\lambda = 10^{-5}$	68.99	<b>49.45</b>	29.51	14.68	6.31		
SNC $\sigma = 10$	68.47	48.74	29.07	14.32	6.04		
w/o Reg.	68.46	48.77	29.20	14.50	6.08		
CIFAR100		Adversarial training					
Absum $\lambda = 10^{-4}$	<b>42.19</b>	<b>27.25</b>	15.89	<b>8.47</b>	4.14		
WD $\lambda = 10^{-7}$	41.14	27.05	<b>15.90</b>	8.26	<b>4.28</b>		
L1 $\lambda = 10^{-4}$	40.75	26.14	14.45	7.61	3.67		
SNC $\sigma = 10$	40.90	26.61	15.53	8.32	4.13		
w/o Reg.	40.70	26.24	14.85	7.94	3.86		
SVHN		Adversarial training					
Absum $\lambda = 10^{-5}$	<b>77.78</b>	<b>52.74</b>	<b>27.39</b>	11.97	5.50		
WD $\lambda = 10^{-7}$	76.66	50.40	25.05	10.86	5.04		
L1 $\lambda = 10^{-6}$	76.50	51.49	27.10	<b>12.12</b>	<b>5.63</b>		
SNC $\sigma = 1.0$	77.23	50.80	25.24	11.04	5.03		
w/o Reg.	N/A	N/A	N/A	N/A	N/A		

training, Absum improves robustness against PGD, the highest among regularization methods, on almost all datasets. This implies that sensitivity to SFA is one of the causes of vulnerabilities of CNNs. The  $\lambda$  of Absum tends to be higher than the  $\lambda$  of WD and  $L_1$ ; thus, Absum can also improve robustness against PGD without deteriorating classification performance due to its looseness. Note that Absum does not improve robustness against PGD without adversarial training since the structural sensitivity of CNNs does not necessarily cause all vulnerabilities of CNN-based models (we discussed this in the appendix). Even so, Absum is more effective than other standard regularizations since it can efficiently improve robustness against black-box attacks (SFA, transferred attacks, and High-Frequency attacks) and enhance adversarial training, as mentioned above.

## Conclusion

We proposed Absum; an efficient defense method against SFA that can reduce the structural sensitivity of CNNs with ReLUs while its computational cost remains comparable to standard regularizations. By reducing the structural sensitivity, Absum can improve robustness against not only SFA, but also transferred PGD, and High-Frequency attacks. Due to its simplicity, Absum can be used with other methods, and Absum can enhance adversarial training of PGD.

## References

- [Athalye, Carlini, and Wagner 2018] Athalye, A.; Carlini, N.; and Wagner, D. 2018. Obfuscated gradients give a false sense of security: Circumventing defenses to adversarial examples. In *Proc. ICML*, 274–283.
- [Brendel, Rauber, and Bethge 2018] Brendel, W.; Rauber, J.; and Bethge, M. 2018. Decision-based adversarial attacks: Reliable attacks against black-box machine learning models. In *Proc. ICLR*.
- [Carlini and Wagner 2017] Carlini, N., and Wagner, D. 2017. Towards evaluating the robustness of neural networks. In *2017 IEEE Symposium on Security and Privacy (SP)*, 39–57. IEEE.
- [Chen et al. 2017] Chen, P.-Y.; Zhang, H.; Sharma, Y.; Yi, J.; and Hsieh, C.-J. 2017. Zoo: Zeroth order optimization based black-box attacks to deep neural networks without training substitute models. In *Proceedings of the 10th ACM Workshop on Artificial Intelligence and Security*, 15–26. ACM.
- [Cisse et al. 2017] Cisse, M.; Bojanowski, P.; Grave, E.; Dauphin, Y.; and Usunier, N. 2017. Parseval networks: Improving robustness to adversarial examples. In *Proc. ICML*, 854–863.
- [Das et al. 2018] Das, N.; Shanbhogue, M.; Chen, S.-T.; Hohman, F.; Li, S.; Chen, L.; Kounavis, M. E.; and Chau, D. H. 2018. Shield: Fast, practical defense and vaccination for deep learning using jpeg compression. In *Proceedings of the 24th ACM SIGKDD International Conference on Knowledge Discovery & Data Mining*, 196–204. ACM.
- [Dhillon et al. 2018] Dhillon, G. S.; Azizzadenesheli, K.; Lipton, Z. C.; Bernstein, J.; Kossaifi, J.; Khanna, A.; and Anandkumar, A. 2018. Stochastic activation pruning for robust adversarial defense. *Proc. ICLR*.
- [Ding, Wang, and Jin 2019] Ding, G. W.; Wang, L.; and Jin, X. 2019. AdverTorch v0.1: An adversarial robustness toolbox based on pytorch. *arXiv preprint arXiv:1902.07623*.
- [Goodfellow, Bengio, and Courville 2016] Goodfellow, I.; Bengio, Y.; and Courville, A. 2016. *Deep learning*. MIT press.
- [Goodfellow, Shlens, and Szegedy 2014] Goodfellow, I.; Shlens, J.; and Szegedy, C. 2014. Explaining and harnessing adversarial examples. *arXiv preprint arXiv:1412.6572*.
- [Gouk et al. 2018] Gouk, H.; Frank, E.; Pfahringer, B.; and Cree, M. 2018. Regularisation of neural networks by enforcing lipschitz continuity. *arXiv preprint arXiv:1804.04368*.
- [He et al. 2016] He, K.; Zhang, X.; Ren, S.; and Sun, J. 2016. Deep residual learning for image recognition. In *Proc. CVPR*, 770–778.
- [Ilyas et al. 2018] Ilyas, A.; Engstrom, L.; Athalye, A.; and Lin, J. 2018. Black-box adversarial attacks with limited queries and information. In *Proc. ICML*, 2137–2146.
- [Ioffe and Szegedy 2015] Ioffe, S., and Szegedy, C. 2015. Batch normalization: Accelerating deep network training by reducing internal covariate shift. In *Proc. ICML*, 448–456.
- [Jain 1989] Jain, A. K. 1989. *Fundamentals of Digital Image Processing*. Prentice-Hall.
- [Jo and Bengio 2017] Jo, J., and Bengio, Y. 2017. Measuring the tendency of cnns to learn surface statistical regularities. *arXiv preprint arXiv:1711.11561*.
- [Karner, Schneid, and Ueberhuber 2003] Karner, H.; Schneid, J.; and Ueberhuber, C. W. 2003. Spectral decomposition of real circulant matrices. *Linear Algebra and Its Applications* 367:301–311.
- [Krizhevsky and Hinton 2009] Krizhevsky, A., and Hinton, G. 2009. Learning multiple layers of features from tiny images. Technical report.
- [Kurakin, Goodfellow, and Bengio 2016] Kurakin, A.; Goodfellow, I.; and Bengio, S. 2016. Adversarial machine learning at scale. *arXiv preprint arXiv:1611.01236*.
- [LeCun et al. 1989] LeCun, Y.; Boser, B.; Denker, J. S.; Henderson, D.; Howard, R. E.; Hubbard, W.; and Jackel, L. D. 1989. Backpropagation applied to handwritten zip code recognition. *Neural computation* 1(4):541–551.
- [LeCun et al. 1998] LeCun, Y.; Bottou, L.; Bengio, Y.; Haffner, P.; et al. 1998. Gradient-based learning applied to document recognition. *Proceedings of the IEEE* 86(11):2278–2324.
- [Li and Lin 2015] Li, H., and Lin, Z. 2015. Accelerated proximal gradient methods for nonconvex programming. In *Proc. NIPS*, 379–387.
- [Liu et al. 2019] Liu, Z.; Liu, Q.; Liu, T.; Xu, N.; Lin, X.; Wang, Y.; and Wen, W. 2019. Feature distillation: Dnn-oriented jpeg compression against adversarial examples. In *Proc. CVPR*, 860–868.
- [Madry et al. 2018] Madry, A.; Makelov, A.; Schmidt, L.; Tsipras, D.; and Vladu, A. 2018. Towards deep learning models resistant to adversarial attacks. In *Proc. ICLR*.
- [Moosavi-Dezfooli, Fawzi, and Frossard 2016] Moosavi-Dezfooli, S.-M.; Fawzi, A.; and Frossard, P. 2016. Deepfool: a simple and accurate method to fool deep neural networks. In *Proc. CVPR*, 2574–2582.
- [Nair and Hinton 2010] Nair, V., and Hinton, G. E. 2010. Rectified linear units improve restricted boltzmann machines. In *Proc. ICML*, 807–814. Omnipress.
- [Netzer et al. 2011] Netzer, Y.; Wang, T.; Coates, A.; Bissacco, A.; Wu, B.; and Ng, A. Y. 2011. Reading digits in natural images with unsupervised feature learning. In *NIPS Workshop on Deep Learning and Unsupervised Feature Learning*.
- [Papernot et al. 2016] Papernot, N.; McDaniel, P.; Wu, X.; Jha, S.; and Swami, A. 2016. Distillation as a defense to adversarial perturbations against deep neural networks. In *2016 IEEE Symposium on Security and Privacy (SP)*, 582–597. IEEE.
- [Papernot et al. 2017] Papernot, N.; McDaniel, P.; Goodfellow, I.; Jha, S.; Celik, Z. B.; and Swami, A. 2017. Practical black-box attacks against machine learning. In *Proceedings of the 2017 ACM on Asia Conference on Computer and Communications Security*, 506–519. ACM.
- [Papernot, McDaniel, and Goodfellow 2016] Papernot, N.; McDaniel, P.; and Goodfellow, I. 2016. Transferability in



machine learning: from phenomena to black-box attacks using adversarial samples. *arXiv preprint arXiv:1605.07277*.

[Parikh, Boyd, and others 2014] Parikh, N.; Boyd, S.; et al. 2014. Proximal algorithms. *Foundations and Trends® in Optimization* 1(3):127–239.

[Radford, Metz, and Chintala 2016] Radford, A.; Metz, L.; and Chintala, S. 2016. Unsupervised representation learning with deep convolutional generative adversarial networks. *Proc. ICLR*.

[Sedghi, Gupta, and Long 2019] Sedghi, H.; Gupta, V.; and Long, P. M. 2019. The singular values of convolutional layers. In *Proc. ICLR*.

[Srivastava et al. 2014] Srivastava, N.; Hinton, G. E.; Krizhevsky, A.; Sutskever, I.; and Salakhutdinov, R. 2014. Dropout: a simple way to prevent neural networks from overfitting. *Journal of Machine Learning Research* 15(1):1929–1958.

[Szegedy et al. 2013] Szegedy, C.; Zaremba, W.; Sutskever, I.; Bruna, J.; Erhan, D.; Goodfellow, I.; and Fergus, R. 2013. Intriguing properties of neural networks. *arXiv preprint arXiv:1312.6199*.

[Tsuzuku and Sato 2019] Tsuzuku, Y., and Sato, I. 2019. On the structural sensitivity of deep convolutional networks to the directions of fourier basis functions. *Proc. CVPR*.

[Tsuzuku, Sato, and Sugiyama 2018] Tsuzuku, Y.; Sato, I.; and Sugiyama, M. 2018. Lipschitz-margin training: Scalable certification of perturbation invariance for deep neural networks. In *Proc. NIPS*, 6542–6551.

[Vaswani et al. 2017] Vaswani, A.; Shazeer, N.; Parmar, N.; Uszkoreit, J.; Jones, L.; Gomez, A. N.; Kaiser, Ł.; and Polosukhin, I. 2017. Attention is all you need. In *Proc. NIPS*, 5998–6008.

[Wang et al. 2019] Wang, H.; Wu, X.; Yin, P.; and Xing, E. P. 2019. High frequency component helps explain the generalization of convolutional neural networks. *arXiv preprint arXiv:1905.13545*.

[Wen et al. 2016] Wen, W.; Wu, C.; Wang, Y.; Chen, Y.; and Li, H. 2016. Learning structured sparsity in deep neural networks. In *Proc. NIPS*, 2074–2082.

[Xiao, Rasul, and Vollgraf 2017] Xiao, H.; Rasul, K.; and Vollgraf, R. 2017. Fashion-mnist: a novel image dataset for benchmarking machine learning algorithms. *arXiv preprint arXiv:1708.07747*.

[Yin et al. 2019] Yin, D.; Lopes, R. G.; Shlens, J.; Cubuk, E. D.; and Gilmer, J. 2019. A fourier perspective on model robustness in computer vision. *ICML2019 Workshop (accepted in NeurIPS2019)*.

[Yoshida and Miyato 2017] Yoshida, Y., and Miyato, T. 2017. Spectral norm regularization for improving the generalizability of deep learning. *arXiv preprint arXiv:1705.10941*.

[Yuan et al. 2019] Yuan, X.; He, P.; Zhu, Q.; and Li, X. 2019. Adversarial examples: Attacks and defenses for deep learning. *IEEE transactions on neural networks and learning systems*.

## Appendix

### Proofs of Lemmas

In this section, we provide the proofs of the lemmas.

**Lemma 3.** If  $\bar{\mathbf{k}} = [\bar{k}_1, \dots, \bar{k}_n]^T \in \mathbf{R}^n$ ,  $g(\bar{\mathbf{k}}) = |\sum_i^n \bar{k}_i|$  is a convex function.

*Proof.* If  $g(\cdot)$  is a convex function, we have  $g(t\mathbf{x} + (1-t)\mathbf{y}) \leq tg(\mathbf{x}) + (1-t)g(\mathbf{y})$ , where  $t \in [0, 1]$  and  $\forall \mathbf{x}, \mathbf{y} \in \mathbf{R}^n$ . Therefore, we investigate  $J = tg(\mathbf{x}) + (1-t)g(\mathbf{y}) - g(t\mathbf{x} + (1-t)\mathbf{y})$ , and if  $J \geq 0$ , we prove the lemma. We have

$$\begin{aligned} J &= t|\sum_i x_i| + (1-t)|\sum_i y_i| - |\sum_i (tx_i + (1-t)y_i)|, \\ &= t|\sum_i x_i| + (1-t)|\sum_i y_i| - |t\sum_i x_i + (1-t)\sum_i y_i|, \end{aligned} \quad (17)$$

since  $t \geq 0$  and  $1-t \geq 0$ . Let  $\alpha = t\sum_i x_i$  and  $\beta = (1-t)\sum_i y_i$ ; thus, we have

$$J = |\alpha| + |\beta| - |\alpha + \beta|. \quad (18)$$

From the triangle inequality, we have  $J \geq 0$ ; thus, this completes the proof.  $\square$

**Lemma 4.** If  $\bar{\mathbf{k}} = [\bar{k}_1, \dots, \bar{k}_n]^T \in \mathbf{R}^n$ ,  $\mathbf{u} \in \mathbf{R}^n$  and  $g(\bar{\mathbf{k}}) = |\sum_i^n \bar{k}_i|$ , we have

$$\begin{aligned} \text{prox}_{\lambda g}(\bar{\mathbf{k}}) &= \arg \min_{\mathbf{u}} \frac{1}{2} \|\mathbf{u} - \bar{\mathbf{k}}\|_2^2 + \lambda |\sum_i^n u_i| \quad (19) \\ &= \begin{cases} \bar{\mathbf{k}} + \lambda \mathbf{1} & \text{if } \sum_i^n \bar{k}_i < -\bar{n}\lambda, \\ \bar{\mathbf{k}} - \frac{\sum_i^n \bar{k}_i}{\bar{n}} \mathbf{1} & \text{if } -\bar{n}\lambda \leq \sum_i^n \bar{k}_i \leq \bar{n}\lambda, \\ \bar{\mathbf{k}} - \lambda \mathbf{1} & \text{if } \sum_i^n \bar{k}_i > \bar{n}\lambda. \end{cases} \quad (20) \end{aligned}$$

*Proof.* For clarity, let  $J = \frac{1}{2} \|\mathbf{u} - \bar{\mathbf{k}}\|_2^2 + \lambda |\sum_i^n u_i|$ . We have three cases; (a)  $\sum_i^n u_i > 0$ , (b)  $\sum_i^n u_i < 0$ , and (c)  $\sum_i^n u_i = 0$ . In (a), we have  $|\sum_i^n u_i| = \sum_i^n u_i$ , and  $\frac{\partial J}{\partial u_i} = u_i - \bar{k}_i + \lambda = 0$  at the optimal point. Therefore,  $u_i = \bar{k}_i - \lambda$ , and the solution becomes  $\mathbf{u} = \bar{\mathbf{k}} - \lambda \mathbf{1}$ . The condition is  $\sum_i^n u_i = \sum_i^n \bar{k}_i - \bar{n}\lambda > 0$ , i.e.,  $\sum_i^n \bar{k}_i > \bar{n}\lambda$ . In (b), we have  $|\sum_i^n u_i| = -\sum_i^n u_i$ , and we can optimize  $J = \frac{1}{2} \|\mathbf{u} - \bar{\mathbf{k}}\|_2^2 - \lambda \sum_i^n u_i$  in the same manner as (a). As a result,  $\mathbf{u} = \bar{\mathbf{k}} + \lambda \mathbf{1}$  if  $\sum_i^n \bar{k}_i < -\bar{n}\lambda$ . In (c),  $|\sum_i^n u_i|$  is non-differentiable, but we can use subgradient  $\mathbf{v}$  such as  $|\sum_i^n z_i| \geq |\sum_i^n u_i| + \mathbf{v}^T(\mathbf{z} - \mathbf{u})$ . Let  $B = \{\mathbf{u} \pm r\mathbf{e}_i | i = 1, \dots, n\}$  where small  $r > 0$  and  $\mathbf{e}_k$  be the standard basis; thus, we have  $M = \max_{\mathbf{z} \in B} |\sum_i^n z_i| = |\sum_i^n u_i \pm r| = r$  when  $|\sum_i^n u_i| = 0$ . As a result,  $\mathbf{v}$  is bounded as  $\|\mathbf{v}\|_\infty \leq \frac{M - |\sum_i^n u_i|}{r} = 1$ . We then have  $\frac{\partial J}{\partial u_i} = u_i - \bar{k}_i + \lambda v_i = 0$ ; thus,  $\mathbf{u} = \bar{\mathbf{k}} - \lambda \mathbf{v}$ . Since  $\|\mathbf{v}\|_\infty \leq 1$ , we have  $-\bar{n}\lambda \leq \lambda \sum_i v_i \leq \bar{n}\lambda$ . Thus, the condition becomes  $-\bar{n}\lambda \leq \sum_i \bar{k}_i \leq \bar{n}\lambda$  since  $\sum_i u_i = \sum_i \bar{k}_i + \lambda \sum_i v_i = 0$ . By substituting  $\mathbf{u} = \bar{\mathbf{k}} - \lambda \mathbf{v}$  into  $J$ , we have  $J = \frac{1}{2} \|\lambda \mathbf{v}\|_2^2$  subject to  $\sum_i v_i = \frac{\sum_i \bar{k}_i}{\lambda}$  and  $\|\mathbf{v}\|_\infty \leq 1$ . Thus, the minimum point is  $v_1 = v_2 = \dots = v_n = \frac{\sum_i \bar{k}_i}{\bar{n}\lambda}$ , i.e.,  $\mathbf{v} = \frac{\sum_i \bar{k}_i}{\bar{n}\lambda} \mathbf{1}$ . Therefore,  $\mathbf{u} = \bar{\mathbf{k}} - \frac{\sum_i \bar{k}_i}{\bar{n}} \mathbf{1}$  is the minimum point when  $-\bar{n}\lambda \leq \sum_i \bar{k}_i \leq \bar{n}\lambda$ . This completes the proof.  $\square$

## Inequality of Induced Norms for Convolution

The  $u + n(v - 1)$ -th singular value of a doubly circulant matrix  $\mathbf{A}$  can be written as  $\sigma_{u,v} = |\sum_{l,m} k_{l,m} \exp(j \frac{2\pi}{n}(ul + vm))|$  (not arranged in descending order), and we have  $\|\mathbf{A}\|_2 = \max_{u,v} \sigma_{u,v} \leq \sum_{l,m} |k_{l,m}| \leq \|\mathbf{A}\|_\infty$ . Therefore, the spectral norm of  $\mathbf{A}$  is bounded above by the induced  $\infty$ -norm as  $\|\mathbf{A}\|_2 \leq \|\mathbf{A}\|_\infty$ .

### $L_2$ Regularization and Induced Norm

In this section, we explain that  $L_2$  regularization (weight decay: WD) can constrain the induced norm of a convolutional layer. The  $L_2$  regularization term of the convolution filter  $\mathbf{K} \in \mathbf{R}^{n \times n}$  is

$$\sum_l^n \sum_m^n k_{l,m}^2. \quad (21)$$

On the other hand, the square of the Frobenius norm of  $\mathbf{A}$  becomes

$$\|\mathbf{A}\|_F^2 = \sum_l^{n^2} \sum_m^{n^2} A_{l,m}^2 = n^2 \sum_l^n \sum_m^n k_{l,m}^2. \quad (22)$$

Therefore, if we use the  $L_2$  regularization, we constrain the Frobenius norm of  $\mathbf{A}$ . In addition, let  $\mathbf{M}$  be  $m \times m$  matrices, we have the following inequalities:

$$\|\mathbf{M}\|_2 \leq \|\mathbf{M}\|_F, \quad (23)$$

$$\frac{\|\mathbf{M}\|_\infty}{\sqrt{m}} \leq \|\mathbf{M}\|_2 \leq \sqrt{m} \|\mathbf{M}\|_\infty, \quad (24)$$

where  $\|\cdot\|_2$  is the induced 2-norm, which is the largest singular value. From the above inequalities, we have  $\frac{\|\mathbf{A}\|_\infty}{n} \leq \|\mathbf{A}\|_2 \leq \|\mathbf{A}\|_F$ , and thus, if we decrease the Frobenius norm of  $\mathbf{A}$ , the induced 2-norm and  $\infty$ -norms are also decreased.

### Algorithm of Absum

Algorithm 1 shows the whole training algorithm of Absum. First, we update parameters by SGD (lines 3 and 4). Next, we apply the proximal operator to each convolution filter (lines 5-13). These processes are iteratively performed.

### Related Work

Adversarial attacks are divided into two types; white-box and black-box attacks. The fast gradient sign method (FGSM) and PGD are popular as simple and sophisticated white-box attacks, respectively (Goodfellow, Shlens, and Szegedy 2014; Kurakin, Goodfellow, and Bengio 2016; Madry et al. 2018). Though many defense methods against white-box attacks have been proposed, e.g., defensive distillation (Papernot et al. 2016) and stochastic defense (Dhillon et al. 2018), several methods have been toppled by strong attacks (Athalye, Carlini, and Wagner 2018; Carlini and Wagner 2017). A promising method is adversarial training (Goodfellow, Shlens, and Szegedy 2014; Kurakin, Goodfellow, and Bengio 2016; Madry et al. 2018), which uses adversarial examples as training data. However, its computational cost is larger than naive training. Note that Absum can be used with adversarial training and enhances it, as discussed in experiments. Black-box attacks are more practical than white-box attacks since it is difficult to access the

### Algorithm 1 Training with Absum

---

```

1: Initialize parameters  $\theta$ 
2: while  $e \leq E$  do
3:   Sample a minibatch  $\{(\mathbf{X}_i, \mathbf{Y}_i)\}^B$ 
4:    $\theta \leftarrow \theta - \eta \nabla_{\theta} \frac{1}{B} \sum_b f(\theta, \mathbf{X}_b, \mathbf{Y}_b)$ 
5:   for  $i \in 1, \dots, L$  do
6:     if  $\sum_l^h \sum_m^h k_{l,m}^{(i)} < -h^2 \eta \lambda$  then
7:        $\bar{k}^{(i)} + \eta \lambda \mathbf{1}$ 
8:     else if  $-h^2 \eta \lambda \leq \sum_l^h \sum_m^h k_{l,m}^{(i)} \leq h^2 \eta \lambda$  then
9:        $\bar{k}^{(i)} - \frac{\sum_l^h \sum_m^h k_{l,m}^{(i)}}{h^2} \mathbf{1}$ 
10:    else  $\{\sum_l^h \sum_m^h k_{l,m}^{(i)} > h^2 \eta \lambda\}$ 
11:       $\bar{k}^{(i)} - \eta \lambda \mathbf{1}$ 
12:    end if
13:  end for
14:   $e = e + 1$ 
15: end while

```

---

target models in online applications (Papernot et al. 2017; Yuan et al. 2019). Most black-box attacks are transferred white-box attacks and can be defended against by adversarial training (Papernot et al. 2017). Several black-box attacks use queries that ask the target model about the predicted labels of given input data, but these attacks might still be impractical since they require a large amount of queries (Brendel, Rauber, and Bethge 2018; Chen et al. 2017; Ilyas et al. 2018). On the other hand, SFA only uses the information that the target model is composed of CNNs and is more practical.

An early study (Szegedy et al. 2013) showed that the induced norm can be a measure of robustness, and Parseval networks constrain the induced norm of linear layers to improve robustness (Cisse et al. 2017). Parseval networks are more robust against FGSM than naive models and can enhance adversarial training. However, the computational cost of Parseval networks is larger than standard regularization methods. In addition, its robustness might be less than that of the spectral norm regularization (Tsuzuku, Sato, and Sugiyama 2018) though Parseval networks penalize the spectral norm like the spectral norm constraint. The spectral norm regularization can improve generalization performance (Yoshida and Miyato 2017). However, the spectral norm in spectral norm regularization is often quite different from that of  $\mathbf{A}$  (Gouk et al. 2018; Sedghi, Gupta, and Long 2019) for convolution.

As simple regularization methods, Srivastava et al. (2014) shows that maxnorm regularization can improve generalization performance of deep learning. The maxnorm regularization in (Srivastava et al. 2014) restricts the  $L_2$  norm of weight vectors to be strictly less than or equal to a threshold  $c$  as  $\|\mathbf{A}_i\|_2 \leq c$  where  $\mathbf{A}_i$  is the  $i$ -th row vector of  $\mathbf{A}$  in eq. (5). Therefore, the maxnorm regularization on convolution is  $\|\mathbf{A}_i\|_2 = \sqrt{\sum_l \sum_m k_{l,m}^2} \leq c$  and is similar to  $L_2$  regularization. In fact, we observed that the effectiveness of maxnorm regularization is similar to weight decay.

## Experimental Conditions

We had roughly two experimental conditions according to the dataset. In all experiments, we selected the best regularization weight from among  $[10^1, 10^0, \dots, 10^{-6}, 10^{-7}]$  for Absum and standard regularization methods and selected the best spectral norm  $\sigma$  from among  $[0.01, 0.1, 0.5, 1.0, 10]$  for spectral norm constraint (SNC) (Sedghi, Gupta, and Long 2019). In SNC, we clipped singular values once in 100 iterations due to the large computational cost. Our experiments ran once for each hyperparameter. We assumed that all images were divided by 255 and pixels had the values between 0 and 1. In addition, MNIST, CIFAR10 and CIFAR100 were standardized as (mean, standard deviation)=(0,1) before the images were applied to the models as preprocessing. In the evaluation of robustness, we standardized input images by using the means and standard deviations of clean data after adversarial perturbation. The computation graph of the standardization was preserved in gradient-based attacks; thus, perturbations of PGD were optimized while considering this preprocess.

### MNIST and Fashion-MNIST

The training set of each dataset contains 60,000 examples, and the test set contains 10,000 examples (LeCun et al. 1998; Xiao, Rasul, and Vollgraf 2017). For MNIST and Fashion-MNIST (FMNIST), we stacked two convolutional layers and two fully connected layers, the first convolutional layer had the 10 output channels and the second convolutional layer had 20 output channels. The kernel sizes of the convolutional layers were 5, their strides were 1, and we did not use zero-padding in these layers. After each convolutional layer, we applied max pooling (the stride was 2) and ReLU activation. The output of the second convolutional layer was applied to the first fully connected layer (the size was  $320 \times 50$ ), and we used the ReLU activation after the first fully connected layer. The size of the second fully connected layer was  $50 \times 10$ , and we used softmax as the output function. After the second convolution layer and before the second fully connected layer, we applied 50 % dropout. We trained the model for 100 epochs by using Momentum SGD (the learning rate of 0.01 and momentum of 0.5). We set the minibatch size to 64.

We changed  $(l, m)$  to  $\{(0, 0), (0, 1), \dots, (27, 26), (27, 27)\}$  in SFA since the size of the images was  $28 \times 28$  and evaluated the accuracy of the model on the test data perturbed by SFA. The  $L_\infty$  norm of the perturbation of SFA was set to  $80/255$ . The perturbed inputs were clipped so that each element would be included in  $[0, 1]$ . For fair comparison, all regularization methods were applied to only convolution filter parameters.

### CIFAR10, CIFAR100, and SVHN

CIFAR10 and CIFAR100 contain 50,000 training images and 10,000 test images (Krizhevsky and Hinton 2009). SVHN contains 73,257 images for training and 26,032 images for testing (Netzer et al. 2011). For SVHN, we used cropped digits, which were cropped as  $32 \times 32$ . The model architecture was ResNet-18 for CIFAR10, CIFAR100, and

SVHN (He et al. 2016).<sup>4</sup> As the preprocessing for training, given images were randomly cropped as  $32 \times 32$  after padding a sequence of four on each border of the images. Horizontal flip was randomly applied to images with a probability of 0.5. We trained the model for 350 epochs with Momentum SGD (momentum 0.9). The initial learning rate was set to 0.1, and after 150 and 250 epochs, we divided the learning rate by 10. We set the minibatch size to 128.

We changed  $(l, m)$  in SFA to  $\{(0, 0), (0, 1), \dots, (31, 30), (31, 31)\}$  since the size of the images was  $32 \times 32$  and evaluated the accuracy of the model on the test data perturbed by SFA. The  $L_\infty$  norm of the perturbation of SFA was set to  $10/255$ . The perturbed inputs were clipped so that each element would be included in  $[0, 1]$ . For fair comparison, all regularization methods were applied to only convolution filter parameters.

Note that about 20 % of SVHN test and train datasets have the class label of ‘1’. Due to the class imbalance, models output class ‘1’ regardless of input images in some hyperparameter settings. In this case, the robust accuracies are always about 20%; thus, these models sometimes outperform properly trained models with naive training in terms of robust accuracy. However, these results are not meaningful, and we do not list them in the tables. For the other datasets, we also do not list the results of the models that output one class regardless of input images.

### High-Frequency Attack

To evaluate robustness in the frequency domain, we used High-Frequency attacks. High-Frequency attacks can be regarded as low-pass filteres, which remove high-frequency components. In High-Frequency attacks (Wang et al. 2019), we first apply discrete Fourier transform (DFT)  $\mathcal{F}$  to data  $\mathbf{X}$  as

$$\mathbf{Z} = \mathcal{F}(\mathbf{X}). \quad (25)$$

Next, we decompose the low- and high-frequency components as

$$Z_{i,j}^l = \begin{cases} Z_{i,j} & \text{if } d((i, j), (c_i, c_j)) \leq r \\ 0 & \text{otherwise} \end{cases}, \quad (26)$$

$$Z_{i,j}^h = \begin{cases} 0 & \text{if } d((i, j), (c_i, c_j)) \leq r \\ Z_{i,j} & \text{otherwise} \end{cases}, \quad (27)$$

where  $Z_{i,j}^l$  and  $Z_{i,j}^h$  are elements of low- and high-frequency components in the frequency domain, respectively,  $(c_i, c_j)$  is a centroid of the image,  $d(\cdot, \cdot)$  is the Euclidean distance, and  $r$  is a radius that determines the cutoff frequency. Finally, we apply the inverse DFT to  $\mathbf{Z}^l$  as

$$\mathbf{X}^l = \mathcal{F}^{-1}(\mathbf{Z}^l), \quad (28)$$

and  $\mathbf{X}^l$  is an input image attacked by High-Frequency attacks. While  $r$  is gradually reduced and accuracies are iteratively evaluated for each  $r$  in (Wang et al. 2019), we used fixed  $r$  as half of the image width since we just focus on comparing Absum with other methods.

<sup>4</sup>Our training settings are based on the open source of <https://github.com/kuangliu/pytorch-cifar>.

In addition to High-Frequency attacks, we evaluated robust accuracies against high-pass filter  $\mathbf{X}^h = \mathcal{F}^{-1}(\mathbf{Z}^h)$ . Note that images processed by the high-pass filter are not adversarial examples since it is difficult for humans to accurately classify these images. Even so, this experiment reveals how the model trained using each method is biased towards the low-frequency components.

### Computational Cost

We evaluated the computation time of Absum. We used one NVIDIA Tesla V100 GPU and 32 Intel(R) Xeon(R) Silver 4110 CPUs, and our implementation used Python 3.6.8, pytorch 0.4.1, CUDA 9.0, and numpy 1.11.3 in this experiment. Note that we used numpy to compute the FFT and singular value decomposition, which is difficult to parallelize, in SNC. We clipped singular values once in 100 iterations due to the large computational cost. The model architectures and training process were the same as those of the experiments involving SFA. We used  $\lambda = 10^{-4}$  and  $\sigma = 1.0$ . We also conducted an experiment to evaluate the computational time when the input size increases. We generated random images whose sizes were  $3 \times 32 \times 32$ ,  $3 \times 64 \times 64$ ,  $3 \times 128 \times 128$ ,  $3 \times 256 \times 256$ ,  $3 \times 512 \times 512$ , and  $3 \times 1024 \times 1024$  with ten random labels, and evaluated the computation time of the forward and backward processes of ResNet18 for one image.

### Robustness against PGD

We also evaluated the effectiveness of Absum against PGD. We evaluated Absum with adversarial training (Madry et al. 2018) in addition to naive training because Absum and other regularization methods can be used with adversarial training. In these experiments, we used advtorch (Ding, Wang, and Jin 2019) to generate adversarial examples of PGD.

Model architectures and training conditions were almost the same as the experiments of SFA. The number of epochs for MNIST and FMNIST was set to 100. On the other hand, we observed overfitting in the adversarial training on CIFAR10, CIFAR100, and SVHN. Therefore, we trained the model for 150 epochs with Momentum SGD (momentum 0.9). The initial learning rate was set to 0.1, and after 50 and 100 epochs, we divided the learning rate by 10. We also applied weight decay of  $10^{-4}$  to all parameters on CIFAR10 and CIFAR100 in the adversarial training of PGD since overfitting easily occurred in adversarial training on these datasets.

In PGD, the  $L_\infty$  norm of the perturbation  $\varepsilon$  was set to  $\varepsilon = [0.05, 0.1, 0.15, 0.2, 0.25, 0.4]$  for MNIST and FMNIST, and  $\varepsilon = [4/255, 8/255, 12/255, 16/255, 20/255]$  for CIFAR10 at evaluation time. For PGD, we updated the perturbation for 40 iterations with a step size of 0.01 on MNIST and FMNIST at training and evaluation times. On CIFAR10, CIFAR100, and SVHN, we updated the perturbation for 7 iterations with a step size of  $2/255$  at training time and 100 iterations at evaluation time. The starting points of PGD were randomly initialized from a uniform distribution of  $[-2/255, 2/255]$ . For adversarial training, we used training data perturbed by PGD with  $\varepsilon = 0.3$  on MNIST and  $\varepsilon = 8/255$

on CIFAR10, CIFAR100, and SVHN. In adversarial training, we only used adversarial examples of training data. The above conditions are based on (Madry et al. 2018).

## Additional Experimental Results

### Robustness against SFA

Figure 8 shows the accuracies on datasets perturbed by SFA against hyperparameters  $(l, m)$  of SFA. As shown in Fig. 8, the models trained with WD and  $L_1$  regularization are sensitive to certain frequency noise (e.g., (17, 17) in Figs. 8 (j) and (k)). Table 5 lists the average, minimum, and clean accuracies on datasets perturbed by SFA. In this table, Avg. denotes accuracies on data perturbed by SFA averaged over hyperparameters  $(l, m)$ , and Min. denotes minimum accuracies on data perturbed by SFA among  $(l, m)$ . CLN denotes accuracies on clean data. The  $\lambda$  and  $\sigma$  are selected for each of Avg., Min., and CLN so that each of them would become the highest.

Figure 9 shows the accuracies of the methods on FMNIST, CIFAR100, and SVHN perturbed by SFA against regularization weights. These results are almost the same as those of MNIST and CIFAR 10. On all the datasets, Absum improves the avg. and min. accuracies according to the regularization weights, while the other methods decrease the accuracies according to them.

Figure 10 shows the accuracies of SNC on all datasets perturbed by SFA against the threshold of the spectral norm  $\sigma$ . We can see that, on MNIST and FMNIST, accuracies increase along with  $\sigma$ . This is because, when the spectral norm is small, gradient vanishing occurs in the stacked convolutional layers. On the other hand, on CIFAR10, CIFAR100, and SVHN, where we used ResNet, minimum accuracy decreases, when the spectral norm becomes larger than a certain point, while max accuracy increases along with the spectral norm. Figure 11 shows the lowest training loss  $\frac{1}{N}f$  in training with SNC on CIFAR10 against  $\sigma$ . We can see that SNC with low  $\sigma$  prevents the minimizing of the loss function.

### Robustness against Transferred PGD

Table 6 lists robust accuracies against transferred PGD for various  $\varepsilon$ . We can see that Absum and SNC can improve robustness against transferred PGD better than WD and  $L_1$ .

### Accuracy on Data Filtered using High-pass Filter

Table 7 lists accuracies on test data processed using the high-pass filter. As shown in this table, the accuracies of Absum tend to be higher than the other methods. This table and results against High-Frequency attacks imply that Absum does not bias towards a specific frequency domain. On the other hand, the models trained using SNC are not more robust against the high-pass filter than WD and  $L_1$  while they are more robust against High-Frequency attacks. Therefore, SNC biases CNNs towards low-frequency components of image data.

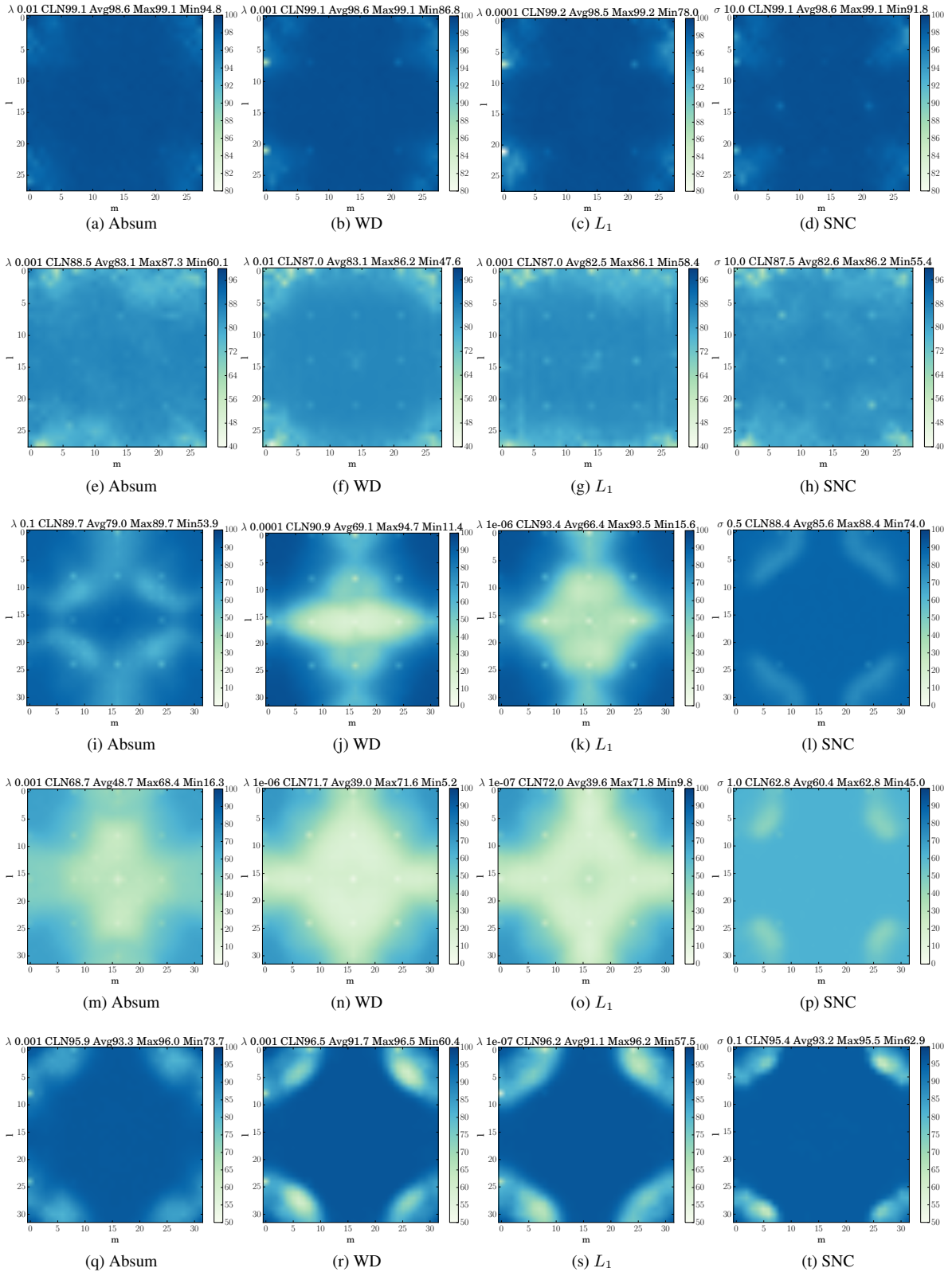
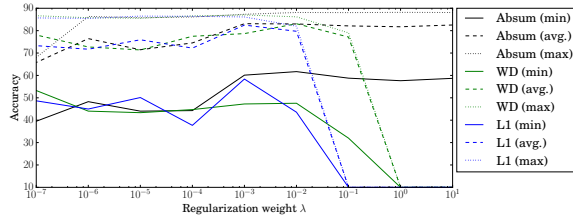


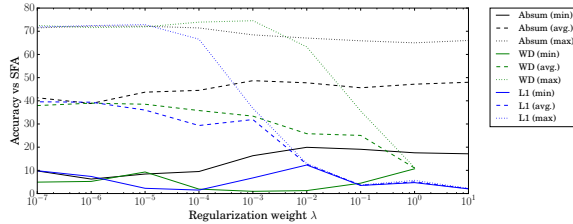
Figure 8: Accuracies of methods on MNIST (a)-(d), FMNIST (e)-(h), CIFAR10 (i)-(l), CIFAR100 (m)-(p), and SVHN (q)-(t) perturbed by SFA ( $l, m$ ). CLN is accuracy on clean data.  $\lambda$  and  $\sigma$  are selected so that average accuracies (Avg) against SFA would achieve largest values.

Table 5: Accuracies of each method on datasets perturbed by SFA ( $l, m$ ).  $\lambda$  and  $\sigma$  are selected so that each accuracy would be highest.

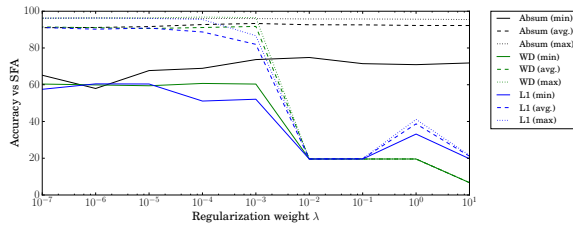
	Avg.					Min.					CLN				
	Absum	WD	L1	SNC	w/o Reg.	Absum	WD	L1	SNC	w/o Reg.	Absum	WD	L1	SNC	w/o Reg.
MNIST	<b>98.64</b>	98.59	98.48	98.55	98.44	<b>95.25</b>	94.65	91.61	91.79	80.53	<b>99.23</b>	99.21	99.19	99.10	99.18
FMNIST	<b>83.11</b>	83.09	82.49	82.60	72.75	<b>60.12</b>	53.25	58.38	55.36	42.92	89.25	89.20	89.27	87.50	<b>89.37</b>
CIFAR10	79.05	69.09	66.44	<b>85.57</b>	66.64	53.90	20.80	29.82	<b>73.99</b>	11.74	93.87	<b>94.73</b>	93.78	93.51	93.53
CIFAR100	48.69	42.97	38.99	<b>60.42</b>	39.52	19.94	10.67	12.31	<b>45.58</b>	8.89	72.38	<b>74.63</b>	73.02	71.51	71.93
SVHN	<b>93.34</b>	91.74	91.14	93.20	90.72	<b>74.83</b>	70.77	60.70	70.66	58.48	96.27	<b>96.72</b>	96.20	96.15	96.17



(a) FMNIST



(b) CIFAR100



(c) SVHN

Figure 9: Accuracies of methods on dataset perturbed by SFA vs regularization weight

### Computational Cost

We evaluated the computation time for convergence on CIFAR10. Figure 12 shows the training loss  $\frac{1}{N}f$  against computation time when  $\lambda = 10^{-4}$  and  $\sigma = 1.0$ . In this figure, Absum converges as fast as L1 regularization.

### Robustness against PGD

Table 8 lists the test accuracies of the models trained by naive training and adversarial training on the data perturbed by PGD. We can see that when we train the models without using adversarial training, Absum does not improve robustness against PGD. This implies that the structural sensitivity of CNNs does not necessarily cause all vulnerabilities of CNN-based models. However, when we use adversarial

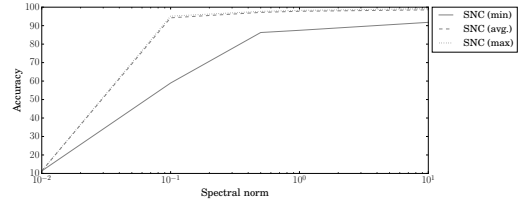
training, Absum improves robustness against PGD, the highest among regularization methods on almost all datasets. Therefore, robustness against Fourier basis functions can contribute to robustness against other adversarial attacks. We can see that SNC can slightly improve the robustness against PGD in naive training. However, when using adversarial training, it does not improve robustness more than Absum. The best regularization weights for WD and L1 regularization in adversarial training tend to be lower, and  $\sigma$  in adversarial training is higher compared with naive training. These results indicate that these methods impose too tight of constraints to achieve high accuracy and robustness at the same time. On the other hand, the best regularization weights of Absum in adversarial training tend to be higher than those in naive training. Thus, Absum can improve robustness without deteriorating classification performance due to its looseness.

Table 6: Accuracies (%) on test datasets perturbed by transferred PGD

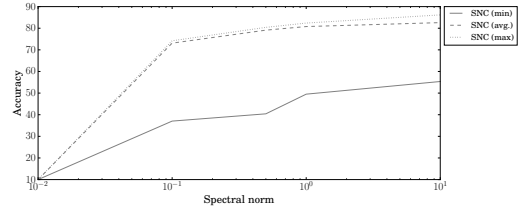
MNIST				
$\varepsilon$	0.10	0.20	0.30	
Absum $\lambda = 10^{-2}$	<b>95.71</b>	<b>76.34</b>	<b>34.39</b>	
WD $\lambda = 10^{-3}$	92.67	48.94	6.63	
L1 $\lambda = 10^{-4}$	94.63	66.48	23.30	
SNC $\sigma = 1.0$	94.99	71.30	25.24	
w/o Reg.	94.68	65.87	25.54	
FMNIST				
Absum $\lambda = 10^{-3}$	<b>58.32</b>	<b>30.08</b>	<b>17.02</b>	
WD $\lambda = 10^{-2}$	35.15	3.46	0.02	
L1 $\lambda = 10^{-3}$	48.47	18.35	7.08	
SNC $\sigma = 10$	51.45	21.31	9.76	
w/o Reg.	39.92	19.74	12.24	
CIFAR10				
$\varepsilon$	2/255	4/255	6/255	
Absum $\lambda = 10^{-1}$	63.33	26.29	8.58	
WD $\lambda = 10^{-4}$	57.45	18.48	5.01	
L1 $\lambda = 10^{-6}$	57.52	15.66	2.88	
SNC $\sigma = 0.5$	<b>74.14</b>	<b>48.85</b>	<b>24.31</b>	
w/o Reg.	57.64	15.85	3.15	
CIFAR100				
Absum $\lambda = 10^{-3}$	41.64	18.57	8.20	
WD $\lambda = 10^{-6}$	42.91	17.40	6.86	
L1 $\lambda = 10^{-7}$	41.35	16.68	6.60	
SNC $\sigma = 1.0$	<b>50.96</b>	<b>36.57</b>	<b>23.90</b>	
w/o Reg.	41.59	16.68	7.28	
SVHN				
Absum $\lambda = 10^{-3}$	78.37	49.11	30.27	
WD $\lambda = 10^{-3}$	76.20	40.49	20.19	
L1 $\lambda = 10^{-7}$	79.99	52.79	32.95	
SNC $\sigma = 1.0$	77.70	46.36	25.78	
w/o Reg.	<b>80.75</b>	<b>54.39</b>	<b>34.17</b>	

Table 7: Robust accuracy against high-pass filter

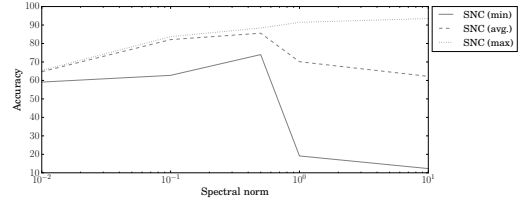
	Absum	WD	L1	SNC	w/o Reg.
MNIST	13.21	40.07	<b>46.96</b>	32.96	27.30
FMNIST	<b>29.75</b>	10.08	10.00	10.05	10.04
CIFAR10	<b>28.75</b>	19.88	20.35	12.93	28.19
CIFAR100	<b>4.03</b>	2.17	1.80	1.1	2.66
SVHN	15.53	<b>19.59</b>	7.50	6.12	6.38



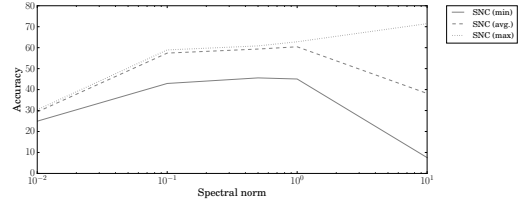
(a) MNIST



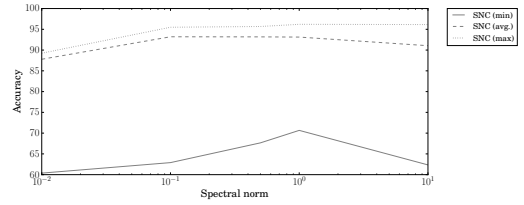
(b) FMNIST



(c) CIFAR10



(d) CIFAR100



(e) SVHN

Figure 10: Accuracies of methods on dataset perturbed by SFA vs spectral norm  $\sigma$  in SNC

Table 8: Accuracies (%) on test datasets perturbed by PGD. Reg. denotes regularization.

MNIST							Adversarial training						
$\varepsilon$	0.05	0.10	0.15	0.20	0.25	0.30	0.05	0.10	0.15	0.20	0.25	0.30	
Naive training							0.05	0.10	0.15	0.20	0.25	0.30	
Absum $\lambda = 10^{-2}$	91.70	58.97	13.30	0.90	0.09	0.00	Absum $\lambda = 10^{-3}$	<b>96.01</b>	<b>94.92</b>	<b>93.75</b>	<b>92.73</b>	<b>91.59</b>	<b>90.78</b>
WD $\lambda = 10^{-5}$	<b>93.38</b>	73.97	34.34	6.55	0.71	0.04	WD $\lambda = 10^{-4}$	92.97	91.34	89.69	88.02	87.05	85.96
L1 $\lambda = 10^{-2}$	92.23	76.02	43.92	13.14	2.29	0.21	L1 $\lambda = 10^{-4}$	93.12	91.86	90.60	89.28	88.25	87.06
SNC $\sigma = 0.5$	92.16	<b>79.30</b>	<b>49.12</b>	<b>16.21</b>	<b>3.64</b>	<b>0.63</b>	SNC $\sigma = 10$	91.92	89.43	86.77	83.89	80.24	76.92
w/o Reg.	93.21	73.81	33.26	6.07	0.70	0.04	w/o Reg.	91.57	89.85	88.43	86.87	85.76	84.86

FMNIST							Adversarial training						
$\varepsilon$	0.05	0.10	0.15	0.20	0.25	0.30	0.05	0.10	0.15	0.20	0.25	0.30	
Naive training							0.05	0.10	0.15	0.20	0.25	0.30	
Absum $\lambda = 10^{-7}$	53.40	21.92	6.19	1.06	0.03	0.00	Absum $\lambda = 10^{-3}$	<b>66.94</b>	<b>65.92</b>	<b>65.77</b>	<b>65.52</b>	<b>65.24</b>	<b>64.95</b>
WD $\lambda = 10^{-2}$	<b>54.45</b>	<b>26.12</b>	8.93	2.19	0.38	0.01	WD $\lambda = 10^{-5}$	65.38	63.64	62.91	62.60	62.11	61.96
L1 $\lambda = 10^{-3}$	52.80	22.43	6.80	1.59	0.18	0.00	L1 $\lambda = 10^{-6}$	66.13	64.16	62.95	62.23	61.64	61.66
SNC $\sigma = 1.0$	49.08	24.03	<b>9.36</b>	<b>3.06</b>	<b>0.68</b>	<b>0.07</b>	SNC $\sigma = 10$	51.58	49.33	47.31	45.85	44.86	44.04
w/o Reg.	52.75	20.97	5.79	0.98	0.05	0.0	w/o Reg.	63.36	61.66	61.15	60.97	60.46	60.26

CIFAR10						Adversarial training					
$\varepsilon$	4/255	8/255	12/255	16/255	20/255	4/255	8/255	12/255	16/255	20/255	
Naive training						4/255	8/255	12/255	16/255	20/255	
Absum $\lambda = 10^{-7}$	0.26	0.00	0.00	0.00	0.00	Absum $\lambda = 10^{-5}$	69.42	49.39	<b>30.22</b>	<b>15.03</b>	<b>6.54</b>
WD $\lambda = 10^{-2}$	8.42	<b>1.87</b>	<b>0.37</b>	0.09	0.02	WD $\lambda = 10^{-5}$	<b>69.48</b>	49.38	29.37	14.45	6.06
L1 $\lambda = 10^{-1}$	5.61	1.43	0.32	<b>0.12</b>	<b>0.08</b>	L1 $\lambda = 10^{-5}$	68.99	<b>49.45</b>	29.51	14.68	6.31
SNC $\sigma = 0.5$	<b>13.39</b>	0.41	0.01	0.00	0.00	SNC $\sigma = 10$	68.47	48.74	29.07	14.32	6.04
w/o Reg.	0.17	0.00	0.00	0.00	0.00	w/o Reg.	68.46	48.77	29.20	14.50	6.08

CIFAR100						Adversarial training					
$\varepsilon$	4/255	8/255	12/255	16/255	20/255	4/255	8/255	12/255	16/255	20/255	
Naive training						4/255	8/255	12/255	16/255	20/255	
Absum $\lambda = 10^{-7}$	2.85	0.35	0.08	0.04	0.02	Absum $\lambda = 10^{-4}$	<b>42.19</b>	<b>27.25</b>	15.89	<b>8.47</b>	4.14
WD $\lambda = 10^{-4}$	4.61	1.08	0.37	0.19	0.14	WD $\lambda = 10^{-7}$	41.14	27.05	<b>15.90</b>	8.26	<b>4.28</b>
L1 $\lambda = 10^{-2}$	4.26	1.53	0.68	<b>0.37</b>	<b>0.17</b>	L1 $\lambda = 10^{-4}$	40.75	26.14	14.45	7.61	3.67
SNC $\sigma = 1.0$	<b>7.03</b>	<b>1.88</b>	<b>0.70</b>	0.25	0.15	SNC $\sigma = 10$	40.90	26.61	15.53	8.32	4.13
w/o Reg.	2.02	0.14	0.03	0.03	0.01	w/o Reg.	40.03	25.42	13.94	7.34	3.68

SVHN						Adversarial training					
$\varepsilon$	4/255	8/255	12/255	16/255	20/255	4/255	8/255	12/255	16/255	20/255	
Naive training						4/255	8/255	12/255	16/255	20/255	
Absum $\lambda = 10^{-7}$	9.36	0.33	0.02	0.00	0.00	Absum $\lambda = 10^{-5}$	<b>77.78</b>	<b>52.74</b>	<b>27.39</b>	11.97	5.50
WD $\lambda = 10^{-4}$	10.46	0.41	0.02	0.00	0.00	WD $\lambda = 10^{-7}$	76.66	50.40	25.05	10.86	5.04
L1 $\lambda = 10^{-5}$	11.78	0.565	0.03	0.00	0.00	L1 $\lambda = 10^{-6}$	76.50	51.49	27.10	<b>12.12</b>	<b>5.63</b>
SNC $\sigma = 0.5$	<b>22.34</b>	<b>2.32</b>	<b>0.21</b>	<b>0.02</b>	<b>0.00</b>	SNC $\sigma = 1.0$	77.23	50.80	25.24	11.04	5.03
w/o Reg.	8.44	0.28	0.02	0.00	0.00	w/o Reg.	N/A	N/A	N/A	N/A	N/A

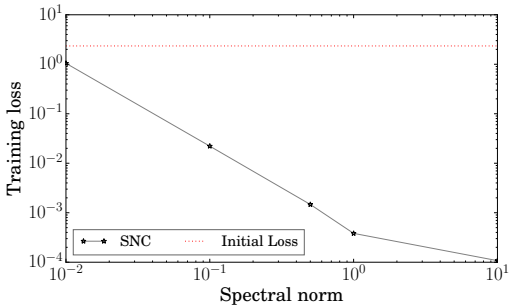


Figure 11: Training loss vs.  $\sigma$  on CIFAR10

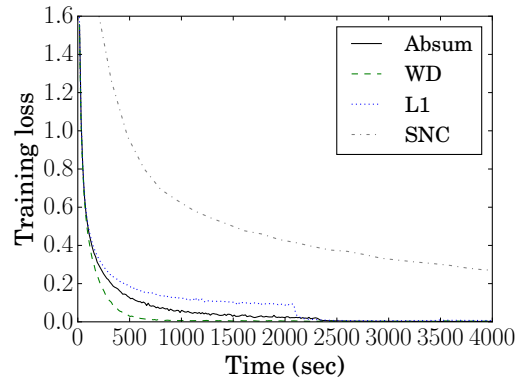


Figure 12: Training loss vs. computation time